Available online at www.sciencedirect.com
SCIENCE DIRECT®
International Journal of Mechanical Sciences 47 (2005) 1423–1441
International Journal of MECHANICAL SCIENCES
www.elsevier.com/locate/ijmecsci

# An internal state variable plasticity-based approach to determine dynamic loading history effects on material property in manufacturing processes

Y.B. Guo[a,*], Q. Wen[a], M.F. Horstemeyer[b]

[a]*Department of Mechanical Engineering, University of Alabama, Tuscaloosa, AL 35487, USA*
[b]*Department of Mechanical Engineering, Mississippi State University, MS 39762, USA*

Received 29 June 2004; received in revised form 25 March 2005; accepted 30 April 2005
Available online 29 June 2005

**Abstract**

Worked materials in large deformation processes such as forming and machining experience a broad range of strain, strain rate, and temperatures, which in turn affect the flow stress. However, the flow stress also highly depends on many other factors such as strain path, strain rate and temperature history. Only a model that includes all of these pertinent factors is capable of predicting complex stress state in material deformation. In this paper, the commonly used phenomenological plasticity models (Johnson–Cook, Usui, etc.) to characterize material behavior in forming and machining were critically reviewed. Although these models are easy to apply and can describe the general response of material deformation, these models lack the mechanisms to reflect static and dynamic recovery and the effects of load path and strain rate history in large deformation processes. These effects are essential to understand process mechanisms, especially surface integrity (residual stress, microhardness, and microstructure) of the manufactured products.

As such a dislocation-based internal state variable (ISV) plasticity model was used, in which the evolution equations enable the prediction of strain rate history and temperature history effects. These effects can be quite large and cannot be modeled by the equation-of-state models that assume that stress is a unique function of the total strain, strain rate, and temperature, independent of the loading path. The temperature dependence of the hardening and recovery functions results in the prediction of thermal softening during adiabatic temperatures rises, which are common in metal forming and machining.

The dynamic mechanical behaviors of three different benchmark work materials, titanium Ti-6Al-4V, AISI 52100 steel (62 HRc), and aluminum 6061-T6, were modeled using the ISV approach. The material

*Corresponding author. Tel.: +1 205 348 2615; fax: +1 205 348 6419.
*E-mail address:* yguo@coe.eng.ua.edu (Y.B. Guo).

0020-7403/$ - see front matter 
doi:10.1016/j.ijmecsci.2005.04.015

**Nomenclature**

| | |
|---|---|
| $\sigma$ | flow stress |
| $K$ | material constant in power law equation |
| $\varepsilon$ | strain |
| $n$ | material constant |
| $A$ | material constant |
| $B$ | material constant in JC model |
| $C$ | material constant in JC model |
| $\dot{\varepsilon}$ | strain rate |
| $\dot{\varepsilon}_0$ | reference strain rate |
| $m$ | material constant |
| $T_h$ | homologous temperature |
| $T$ | temperature |
| $M$ | material constant in Usui model |
| $N$ | material constant in Usui model |
| $k$ | material constant in Usui model |
| $\overset{\circ}{\underline{\sigma}}, \overset{\circ}{\underline{\alpha}}$ | objective rates |
| $\underline{W}$ | continuum spin |
| $\underline{W}^e$ | elastic spin |
| $\lambda, \mu$ | elastic Lame constants |
| $\underline{D}^e$ | elastic rate of deformation |
| $\underline{D}$ | total rate deformation |
| $\underline{D}^{in}$ | inelastic rate of deformation |
| $\underline{\alpha}$ | kinematic hardening internal state variable |
| $R$ | isotropic hardening internal state variable |
| $V(T)$ | magnitude of rate-dependence on yielding at high strain rate |
| $Y(T)$ | yield stress of rate-independent limit |
| $f(T)$ | strain rate at which yield transition from rate-independent to rate-dependent |
| $h(T)$ | anisotropic hardening modulus |
| $H(T)$ | isotropic hardening modulus |
| $r_d(T)$ | dynamic recovery |
| $R_d(T)$ | dynamic recovery |
| $r_s(T)$ | diffusion-controlled static or thermal recovery |
| $R_s(T)$ | diffusion-controlled static or thermal recovery |
| $C_0$–$C_{20}$ | material constants in BCJ model |
| $\rho$ | material density |
| $C$ | specific heat |

constants were obtained by using a nonlinear regression-fitting algorithm in which the stress–strain curves from the model were correlated to the experiments at different (extreme) temperatures. Then the capabilities of the determined material constants were examined by comparing the predicted material flow stress with the test data at different temperatures, strains, and strain rate history. The comparison

demonstrates that the internal state variable plasticity model can successfully recover dynamic material behavior at various deformation states including the loading path effect. In addition, thermal softening due to adiabatic deformation was also captured by this approach.


*Keywords:* Mechanical behavior; Loading history; BCJ model; Manufacturing process

## 1. Introduction

Forming and machining are major manufacturing operations today in terms of their economic significance. Worked materials in these large deformation processes experience a broad range of strain, strain rate, temperature, and complex loading histories. A fundamental knowledge of dynamic material behavior is essential to understand the process mechanisms, characterize surface integrity, establish optimum operation conditions, and develop new tooling. Material behavior is of utmost importance in both the analytical and numerical models to predict process variables and surface integrity for improving process efficiency and product performance.

In forming and machining processes, a broad range of strains (0.1 and over), strain rates (up to $10^6$ 1/s), and temperatures (up to 1300 °C) may occur. Table 1 gives an overview of typical strains, strain rates and temperatures found in forming and machining processes [1,2]. The deformation state can be very complex. Loading path effects can arise from manufacturing processes where deformation-induced anisotropy is realized in a material or under conditions where nonmonotonic loading sequences are experienced [3]. The loading path effects often play an important role in manufacturing processes and product quality.

It is well known that material flow stress in large deformation processes is a function of strain, strain rate, and temperature. However, the flow stress also highly depends on many other factors such as strain path, strain rate and temperature histories. Only a model that includes all of these pertinent factors is capable of predicting complex stress state in material deformation. A major problem, however, in determining flow stress is the severe deformation together with high temperatures of the workpiece material at high deformation speeds, especially in metal cutting. The intense circumstances under which deformation takes place result in mechanical behavior far removed from that encountered in conventional material tests.

Different methods have been developed to estimate the material behavior in large deformation processes. These methods include low strain rate tension, torsion, and compression tests, in which

Table 1
Typical strains, strain rates, and homologous temperatures ($T_h = T/T_{melt}$) of forming and machining processes

| Process | Strain | Strain rate ($s^{-1}$) | $T_{\text{homologous}}$ |
|---|---|---|---|
| Extrusion | 2–5 | $10^{-1}$–$10^{2}$ | 0.16–0.7 |
| Forging/rolling | 0.1–0.5 | $10^{0}$–$10^{3}$ | 0.16–0.7 |
| Sheet-metal forming | 0.1–0.5 | $10^{0}$–$10^{2}$ | 0.16–0.7 |
| Machining | 1–10[a] | $10^{3}$–$10^{6}$ | 0.16–0.9 |

[a]The strain could be larger in the secondary shear zone.

the strains, strain rates, and temperatures that the work material experiences in manufacturing processes are much higher than those encountered in the traditional static materials tests. Moderate and high strain rate split Hopkinson pressure or torsion bar (SHPB) and machining tests were used to approximate the deformation states in manufacturing processes. Flow stress can be determined by deformation condition or as a function of strain, strain rate, and temperature. Based on the test data, several phenomenological plasticity models including power law model, Johnson-Cook (JC) model [4], Usui model [5], Zerilli model [6], and others have been developed to relate flow stress to plastic strain, strain rate, and/or temperature.

Although the phenomenological models are easy to use and may describe the general response of material deformation, these phenomenological models do not capture history effects of load path and strain rate and incorporate the material static and dynamic recovery; therefore, the microstructure property encountered in forming and machining cannot be modeled. The loading path effects are essential to understand process mechanisms, especially surface integrity of the manufactured products. The critical issues and recent advances in multiscale modeling [7] and thermo-mechanical response [8] of metallic materials have been presented.

In this study, the commonly used phenomenological plasticity models were critically reviewed. A new approach was explored in this paper to incorporate loading path effects by using a dislocation mechanics-based plasticity model (Bammann–Chiesa–Johnson—BCJ model) [9,10]. The model was used for three different work materials widely used in machining and forming operations: titanium Ti-6Al-4V, AISI 52100 steel (62 HRc), and aluminum 6061-T6, which experience complex loading (mechanical and thermal) histories. The obtained material constants of these important alloys provide essential data for future process analysis and simulation of forming and machining using this capable plasticity model.

## 2. Critical assessment of the current materials testing and models

### 2.1. Materials testing methods

Various materials testing methods have been developed to obtain material properties in manufacturing processes. The conventional materials tests such as tension, torsion or compression yield stress–strain responses but the strains, strain rates, and temperatures that the material experiences in forming and machining are usually much higher than those encountered in conventional tests.

Compared with the conventional materials tests such as tension or compression, the SHPB apparatus [11] is used for moderate or high strain-rate material measurements. The concept of SHPB involves the determination of dynamics stresses, strains, or displacements occurring at the end of a bar through observation of the effect some distance away. The SHPB have been adapted to several variations such as tensile testing [12] and torsion testing [13,14]. However, the SHPB for compression tests is capable of achieving high deformation rates ($\sim 10^3\,s^{-1}$). Therefore, the SHPB method is suitable to evaluate the flow stress at moderate strain rates under conditions encountered in manufacturing processes and remains as one popular method to estimate the flow stress.

For material deformations of much higher strain rates, a carefully designed machining test coupled with cutting models [15–18] may provide an effective method for estimating the average flow stress at a range of large strains and high strain rates. While the major disadvantage of a machining test is that the determined flow stress is an average and only valid in the range of large strains and high strain rates in cutting conditions. The determination of flow stress beyond this range, such as in the elastic range or low and moderate strain and strain-rate range, becomes very difficult using a machining test. In addition, only one pair of stress/strain data can be obtained in one machining test. Furthermore, the machining test method coupling with the cutting models is limited to cases of continuous chips.

To overcome the disadvantages associated with conventional materials tests or machining tests, several integrated approaches [16,19] of the combined compression (including SHPB) test and machining test have been developed, in which the compression test is used to obtain material flow stress at low and moderate strains and strain rates, while machining tests for large strains and high strain rates.

### 2.2. Empirical and semi-empirical material models

The power law equation, Eq. (1), had long been the most popular material models for simple deformation processes. However, it does not account for any strain rate or temperature effects. The material constants $K$ and $n$ can be obtained by fitting the equation to material test data.

$$\sigma = K\varepsilon^n. \tag{1}$$

At present, the JC model [4] is very often used in finite element analysis to introduce strain rate and temperature dependence of the flow stress. However, it is generally accepted that the correlation of this equation to experimental data is not satisfactory for many materials. The JC model assumes an independent effect of the strain, strain rate, and the temperature.

$$\sigma = [A + B\,\varepsilon^n]\left[1 + C\,\ln\frac{\dot{\varepsilon}}{\dot{\varepsilon}_0}\right](1 - T_h^m), \tag{2}$$

where $T_h = (T - T_{room})/(T_{melt} - T_{room})$.

A different constitutive model, Eq. (3), mainly used in Japan [5,20–22], was proposed to account for effects of strain, strain rate and temperature on the flow stress in machining:

$$\bar{\sigma} = A(10^{-3}\dot{\bar{\varepsilon}})^M \mathrm{e}^{k\,T}(10^{-3}\dot{\bar{\varepsilon}})^m \left\{\int_{T,\dot{\bar{\varepsilon}}\equiv h(\bar{\varepsilon})} \mathrm{e}^{-k\,T/N}(10^{-3}\dot{\bar{\varepsilon}})^{-m/N}\,\mathrm{d}\bar{\varepsilon}\right\}^N \tag{3}$$

The model parameters are temperature dependent. Although the flow stress is strain path dependent, the history effects of temperature and strain rate are not incorporated.

The empirical equations, which relate flow stress to plastic strain, strain rate, and temperature, are not based on reasoning about the nature of the deformation. Therefore, the model parameters are lacking physical interpretation. Besides, despite their sometimes remarkably good fit to

measured stress–strain curves within certain ranges of strains, strain rates and temperatures, empirical relations have no predictive power beyond the range of deformation conditions and material microstructure.

A semi-empirical model by Zerilli and Armstrong [6] is based on dislocation mechanics to incorporate the effects of strain hardening, strain-rate hardening, and thermal softening. The model provides two different relations for FCC and BCC metals, accounting for different rate-controlling mechanisms for these structures:

$$\sigma = C_0 + C_1 e^{(-C_3 T + C_4 T \ln \dot{\bar{\varepsilon}})} + C_5 \bar{\varepsilon}^n (\text{BCC}), \tag{4}$$

$$\sigma = C_0 + C_2 \bar{\varepsilon}^{0.5} e^{(-C_3 T + C_4 T \ln \dot{\bar{\varepsilon}})} (\text{FCC}). \tag{5}$$

It is remarkable that the dependence of the flow stress on the strain is not affected by temperature or strain rate for BCC materials. In contrast, for FCC materials they consider the strain dependence to be strongly affected by the latter two variables. Compared with the JC model, the accuracy of Zerilli–Armstrong model depends on specific materials [23]. An arbitrary power-law used for BCC materials has much less physical meaning.

The empirical and semi-empirical models for work hardening of metals are not physically based, their usage is limited only to the range of deformation conditions at which they were curve fitted, and the accuracy is often not satisfactory. What is missing in these models is the ability to capture history effects of temperature, strain rate, and load path in manufacturing processes.

## 3. Internal state variable plasticity model

Accurate material behavior prediction during large deformations is essential for process analysis. Manufacturing processes will benefit from a better understanding of and ability to predict material behavior when subjected to high and varying strain rates and temperatures. Incorporation of strain rate, temperature, and deformation path history effects are especially critical to accurately predict material responses. The internal state variable (ISV) plasticity model (BCJ model) by Bammann [9], Bammann, Chiesa, and Johnson [10] (BCJ) was used in this study to model these specific phenomena. The BCJ model incorporates strain rate and temperature sensitivity, as well as damage, through a yield surface approach in which the state variables follow a hardening minus-recovery format. The pertinent equations in this model are denoted by the rate of change of the observable and internal state variables. The equations used are given by

$$\overset{\circ}{\underline{\sigma}} = \dot{\underline{\sigma}} - \underline{W}^e \underline{\sigma} + \underline{\sigma} \underline{W}^e = \lambda tr(\underline{D}^e) \underline{I} + 2\mu \underline{D}^e, \tag{6}$$

$$\underline{D}^e = \underline{D} - \underline{D}^{in}, \tag{7}$$

$$\underline{D}^{in} = f(T) \sin h \left[ \frac{||\underline{\sigma} - \underline{\alpha}|| - \{R + Y(T)\}}{V(T)} \right] \frac{\underline{\sigma} - \underline{\alpha}}{||\underline{\sigma} - \underline{\alpha}||}, \tag{8}$$

$$\overset{\circ}{\underline{\alpha}} = \dot{\underline{\alpha}} - \underline{W}^e\,\underline{\alpha} + \underline{\alpha}\,\underline{W}^e$$
$$= \left\{ h(T)\underline{D}^{in} - \left[ \sqrt{\frac{2}{3}} r_d(T) ||\underline{D}^{in}|| + r_s(T) \right] ||\underline{\alpha}||\,\underline{\alpha} \right\}, \tag{9}$$

$$\dot{R} = \left\{ H(T)\underline{D}^{in} - \left[ \sqrt{\frac{2}{3}} R_d(T) ||\underline{D}^{in}|| + R_s(T) \right] R^2 \right\}. \tag{10}$$

The rate equations are generally written as objective rates ($\overset{\circ}{\underline{\sigma}}, \overset{\circ}{\underline{\alpha}}$) assuming a Jaumann rate in which the continuum spin equals the elastic spin ($\underline{W} = \underline{W}^e$). The ISV Eqs. (9) and (10) are functions of the observable variables (temperature, stress state, and rate of deformation). In general, the rate equations of generalized displacements, or thermodynamics fluxes, describing the rate of change may be written as independent equations for each ISV or as derivatives of a suitably chosen potential function arising from the hypothesis of generalized normality. In Eq. (6), the elastic Lame constants are denoted by $\lambda$ and $\mu$. The elastic rate of deformation ($\underline{D}^e$) results when the flow rule as shown in Eq. (7) is subtracted from the total deformation ($\underline{D}$), which is defined by the boundary conditions.

The independent variables for the inelastic rate of deformation are given in Eq. (8) as the stress, temperature, and internal state variables. The deviatoric inelastic flow rule, $\underline{D}^{in}$, encompasses the regimes of creep and plasticity and is a function of the temperature, the kinematic hardening internal state variable ($\underline{\alpha}$), the isotropic hardening internal state variable ($R$), and the functions $f(T)$, $V(T)$ and $Y(T)$, which are related to yielding with Arrhenius-type temperature dependence. The function $Y(T)$ is the rate-independent yield stress. The function $f(T)$ determines when rate dependence affects the initial yielding. The function $V(T)$ determines the magnitude of rate dependence on yielding. These three functions specify the yield stress. These functions are determined from isothermal compression tests with different strain rates and temperatures.

$$V(T) = C_1 \exp(-C_2/T), \tag{11}$$

$$Y(T) = C_3 \exp(C_4/T) \leftrightarrows ([1 + (\tan h(C_{19}(C_{20} - T)))]/2), \tag{12}$$

$$f(T) = C_5 \exp(-C_6/T). \tag{13}$$

The kinematic-hardening internal state variable $\underline{\alpha}$ reflects the effect of anisotropic dislocation density, and the isotropic-hardening internal state variable $R$ reflects the effect of the global dislocation density. The functions $r_s(T)$ and $R_s(T)$are scalar in nature and describe the diffusion-controlled static or thermal recovery, while $r_d(T)$ and $R_d(T)$ are scalar functions describing dynamic recovery. Hence, the two main types of recovery that are exhibited by populations of dislocations within crystallographic materials are captured in the ISVs. The anisotropic-hardening modulus is $h(T)$, and the isotropic-hardening modulus is $H(T)$. The three parameters $r_d(T)$, $h(T)$, $r_s(T)$ describe the tensor or kinematic hardening and recovery, which can be thought of as the center of yield surface. Finally, $R_d(T), H(T)$, and $R_s(T)$, describe the scalar or isotropic hardening and recovery that can be thought of as the radius of the yield surface.

$$r_d(T) = C_7 \exp(-C_8/T), \tag{14}$$

$$h(T) = C_9 - C_{10}T, \tag{15}$$

$$r_s(T) = C_{11}\exp(-C_{12}/T), \tag{16}$$

$$R_d(T) = C_{13}\exp(-C_{14}/T), \tag{17}$$

$$H(T) = C_{15} - C_{16}T, \tag{18}$$

$$R_s(T) = C_{17}\exp(-C_{18}/T). \tag{19}$$

The BCJ material constants ($C_1 - C_{20}$) can be determined from quasi-static or isothermal compression tests at elevated temperatures. The BCJ model may predict isothermal mechanical behavior and adiabatic material response that is common in metal forming and machining processes. In metal cutting literature, the BCJ model was used to determine the mechanical behavior of ductile iron [24] based on room temperature stress–strain data. However, the temperature-dependent model parameters $r_s(T), R_s(T), r_d(T), R_d(T), h(T)$ and $H(T)$ were simplified as constants.

While the BCJ plasticity model is very powerful in representing material behavior, finding values of the 20 material constants representing a particular material can be a daunting task. A nonlinear least-squares program was developed to fit the BCJ model to measured stress–strain curves at different temperatures and rates so that the material constants can be found though it is not easy [25]. Unlike linear least-squares procedures, nonlinear procedure needs starting values at the parameters to be fit, and unfortunately does not guarantee the absolutely ''best'' fit, but can give a fit that is a ''local'' minimum, so the better the initial values, the quicker or better the fit will be. The capabilities of determined material constants with the BCJ model were demonstrated in the following case studies for three fundamentally different materials, titanium Ti-6Al-4V, AISI 52100 steel (62 HRc), and aluminum 6061-T6.

## 4. Case studies

### 4.1. Titanium Ti-6Al-4V

#### 4.1.1. Material constant estimation

Titanium Ti-6Al-4V is an important material often processed by forging and machining in aerospace industry. The test specimen was finished extruded well-below transus and annealed for 1 h at 1033 K. The chemical composition of Ti-6Al-4V is listed in Table 2. The initial microstructure is in $\alpha + \beta$ phase. SHPB tests were performed to determine the flow stress at five different temperatures, 293, 773, 973, 1173, and 1373 K. The temperatures should be uniform across the testing specimens gave enough heating time while not changing microstructures. Four different strain rates, 800, 1700, 2000, 2500 $s^{-1}$, were used. Isothermal condition was assumed in the SHPB tests. Though strain rate can be up to 2500 $s^{-1}$ in the SHPB tests, temperature increase of the specimens was relatively small since thermal energy can be quickly dissipated into the surrounding environment. In addition, microstructures before and after testing were found to have no changes. SHPB testing is not an ideal isothermal testing, but it is far away from adiabatic

Table 2
Nominal chemical composition (weight %) of Titanium Ti-6Al-4V, AISI 52100 steel, and aluminum 6061-T6

| | | | | | | | | | | | | | | |
|---|---|---|---|---|---|---|---|---|---|---|---|---|---|---|
| Ti-6Al-4V | C | | N | | Al | | V | | Fe | | O | | Ti | |
| | 0.014 | | 0.008 | | 6.1 | | 4.0 | | 0.2 | | 0.15 | | 89.53 | |
| 52100 Steel | C | Mn | P | S | Si | Ni | Cr | Mo | Al | Cu | V | Ti | N | O |
| | 1.02 | 0.34 | 0.009 | 0.005 | 0.28 | 0.06 | 1.52 | 0.02 | 0.024 | 0.05 | 0.005 | 0.002 | 0.0065 | 0.0006 |
| 6061-T6 | Al | Mg | Si | Cu | Cr | | Fe | | Mn | | Ti | | Zn | |
| | 98 | 1.0 | 0.6 | 0.28 | 0.2 | | Max 0.7 | | Max 0.15 | | Max 0.15 | | Max 0.25 | |

Table 3
BCJ material constants of titanium Ti-6Al-4V, AISI 52100 (62 HRc), and aluminum 6061-T6

| BCJ material constants | Materials | | |
|---|---|---|---|
| | Ti-6Al-4V | AISI 52100 | Al 6061-T6 |
| $E$(GPa) | 114 (293 K) | 201 (293 K) | 69 (293 K) |
| | 80 (1373 K) | 100 (1273 K) | 40 (933 K) |
| Possion's ratio | 0.34 (293 K) | 0.28 (293 K) | 0.33 (293 K) |
| | 0.4 (1373 K) | 0.4 (1273 K) | 0.4 (933 K) |
| Density (Kg/m$^3$) | 4430 | 7810 | 2700 |
| Specific Heat (J/KgK) | 610 | 475 | 896 |
| $C_1$ (MPa) | 1 | 1 | 187.46 |
| $C_2$ (K) | 0.2 | 0.2 | 1010 |
| $C_3$ (MPa) | 1570 | 2132 | 35.97 |
| $C_4$ (K) | 10 | 73 | 632.1 |
| $C_5$ (1/s) | 1E-05 | 1E-05 | 1 |
| $C_6$ (K) | 0 | 0 | 0 |
| $C_7$ (1/MPa) | 0.07 | 0.69 | 32.344 |
| $C_8$ (K) | 0 | 0 | 1433 |
| $C_9$ (MPa) | 1866 | 1072 | 988.3 |
| $C_{10}$ (K) | 0.3 | 0.1 | 1.331 |
| $C_{11}$ (s/MPa) | 205 | 1E-07 | 5.4E-06 |
| $C_{12}$ (K) | 0 | 0 | 252.1 |
| $C_{13}$ (1/MPa) | 0.0019 | 0.076 | 2.073E+05 |
| $C_{14}$ (K) | 0 | 0.001 | 6394 |
| $C_{15}$ (MPa) | 619 | 31122 | 85.77 |
| $C_{16}$ (K) | 0.38 | 29.8 | 0.06024 |
| $C_{17}$ (s/MPa) | 0.0005 | 2E-06 | 0.003913 |
| $C_{18}$ (K) | 0 | 0 | 2468 |
| $C_{19}$ | 0.0010992 | 0.003711 | 0.019 |
| $C_{20}$ (K) | 876 | 667 | 770 |

conditions such as metal cutting (strain rate up to $10^6\,s^{-1}$). Compared with other testing methods, SHPB testing is one of best methods at present to estimate dynamic mechanical behavior.

The determination of material constants was demonstrated by a nonlinear least-squares fitting the BCJ model to the stress–strain data of titanium Ti-6Al-4V. The elastic part of the material was defined by the temperature-dependent values of Young's modulus and Poisson's ratio in Table 3.

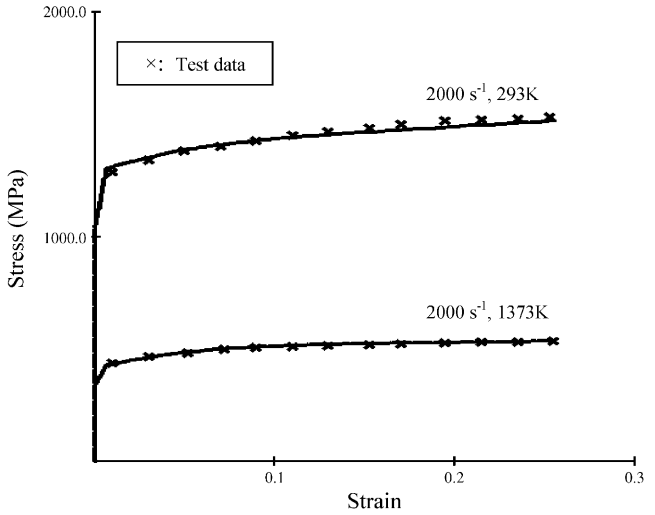


Fig. 1. Determination of BCJ material constants based on test data of Ti-6Al-4V at extreme temperatures.

All the plotted data in the following figures are true stress–true strain obtained from the compression SHPB tests. The isothermal true stress–true strain data at extreme temperatures at 293 and 1373 K [26], Fig. 1, was first used to estimate the BCJ material constants. This was due to two considerations: first, the calculation load can be reduced; second, fitting the extreme temperatures is usually the best approach. The least-squares procedure may not yield "best" fit if fitting all of the parameters at once. It was found that an efficient fitting is to just fit about three parameters while fixing other parameters at a time. The fitting improvement can be monitored by checking the maximum and average residual (fitting errors). Further improvement can be obtained by tuning all parameters until a satisfied fit is found. Parameter study can also be conducted to see the effect of changing a single parameter. Table 3 lists the obtained BCJ material constants for titanium Ti-6Al-4V. It can be seen that a fairly good fit was obtained using the least-squares method.

*4.1.2. Examination of the fitted material constants*

*Stress prediction at different temperatures*: The capability of the BCJ material constants determined at extreme temperatures was demonstrated by the predicted flow stresses, Fig. 2, at different temperatures of 773, 973, and 1173 K. The model predictions agree with the test data very well. For comparison purpose, the stress data used to determine material constants was also shown in Fig. 2.

*Stress prediction at different strain rates*: The predictive capability of BCJ material constants was also verified by comparing the model predictions with the test data, Fig. 3, at different strain rates of 800, 1700, and 2500 $s^{-1}$. The predicted flow stresses also agree with the test data very well.

*Adiabatic effect*: In many applications including forming and machining, deformation occurs rapidly enough (up to $10^6\,s^{-1}$ in machining and $10^3\,s^{-1}$ in forming) that the effects of conduction are negligible. In this situation, the temperature is assumed to increase with the inelastic work. The effect of heating due to plastic work was counted by incorporating a heat generation term

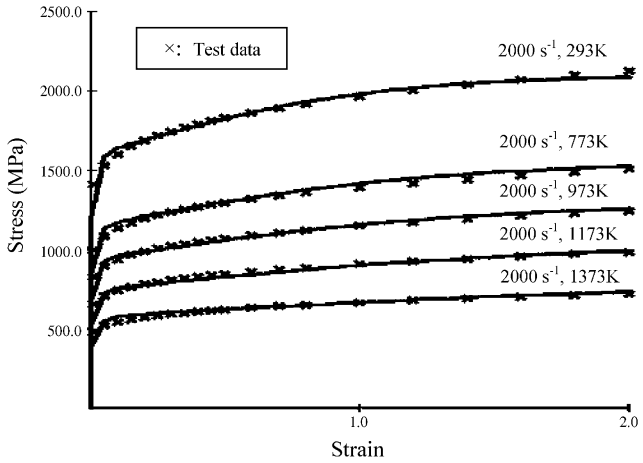


Fig. 2. BCJ model predictions of Ti-6Al-4V at different temperatures.

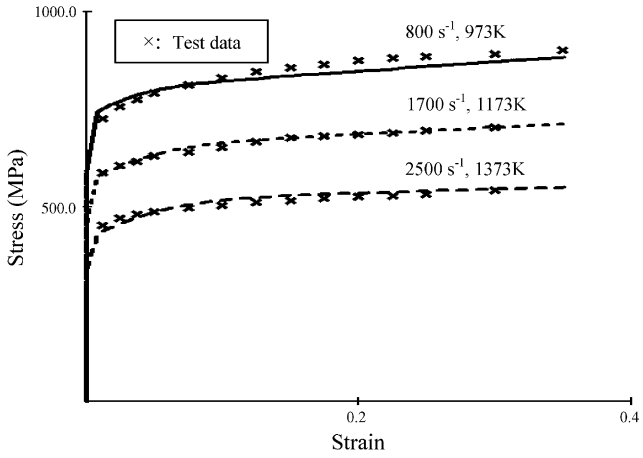


Fig. 3. BCJ model sensitivity to strain rate of Ti-6Al-4V.

$(0.9/\rho C)$, where $\rho$ and $C$ are material density and specific heat, respectively, which are listed in Table 3 for adiabatic calculation. The model predictions for the case of isothermal and adiabatic conditions are given in Figs. 4 and 5. It should be pointed out that the test data of stress–strain in Figs. 4 and 5 was reproduced from Fig. 2. The two figures illustrate that thermal softening occurs at large strains at room temperature and high temperatures, while thermal softening effect is more obvious at the high temperature.

## 4.2. AISI 52100 steel

### 4.2.1. Material constant estimation

In the past decade, hard machining, i.e., machining hardened steels over 35 HRC, has been gaining wide applications in automotive and aerospace industries. For example, AISI 52100 steel

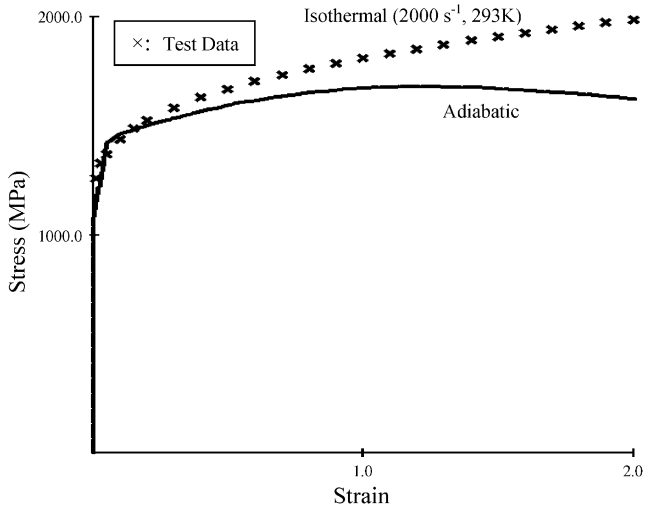


Fig. 4. Adiabatic curve by the BCJ model at 293 K of Ti-6Al-4V.

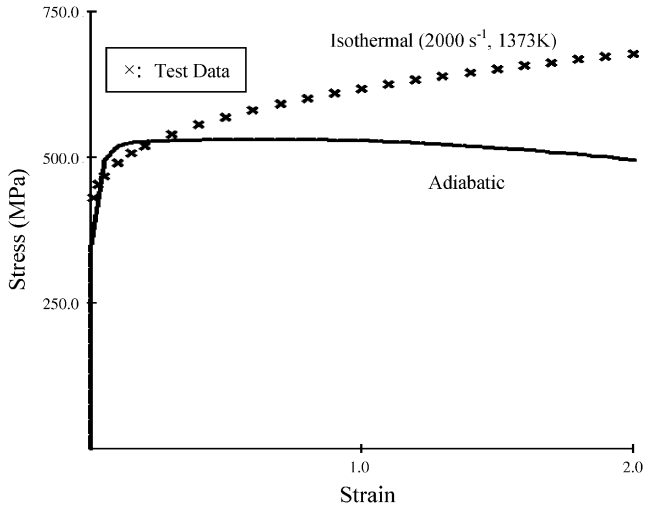


Fig. 5. Adiabatic curve by the BCJ model at 1373 K of Ti-6Al-4V.

(62 HRc) is often used in hard machining to make various precision components such as bearings, shafts, axles, etc. In this work, AISI 52100 cold finished, spheriodized and annealed bars of Brinell hardness 183 were austenized at temperature of 1088 K for 2 h, quenched in oil at 338 K for 15 min, and then tempered at 450 K for 2 h. The measured average hardness (external surface and inside across the diameter) for each sample is 63.08 HRc with a standard deviation of 0.28. Table 2 lists the nominal chemical composition of this material before heat treatment. The heat-treated specimen microstructure includes 96.6% tempered martensite and 3.4% retained austenite. Quasi-static compression tests at elevated temperatures were conducted to obtain the isothermal

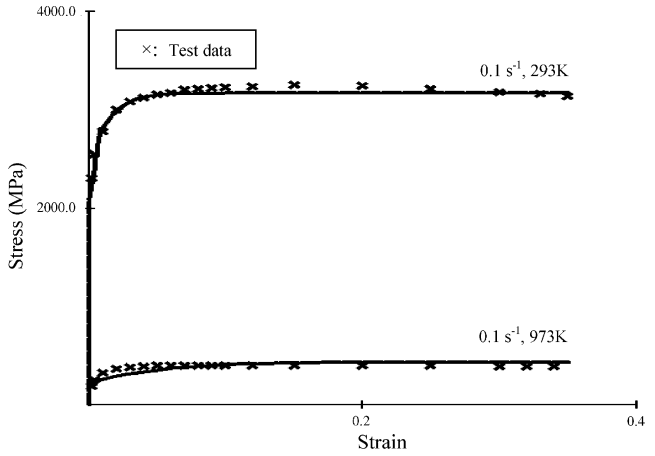


Fig. 6. Determination of BCJ material constants based on test data of AISI 52100 (62 HRc) steel at extreme temperatures.

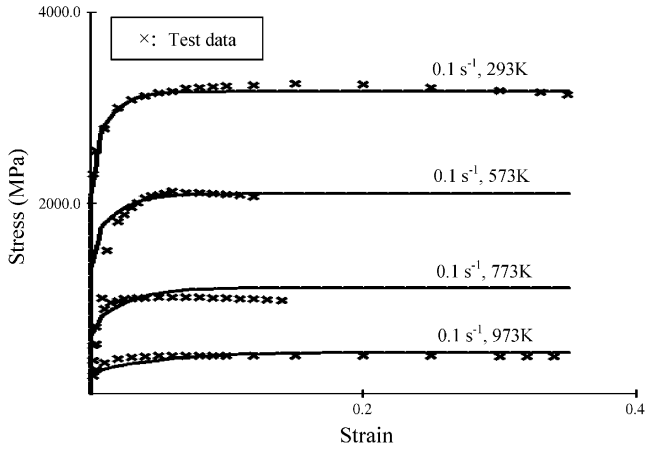


Fig. 7. BCJ model predictions of AISI 52100 (62 HRc) steel at different temperatures.

stress–strain data. The temperature-dependent Young's modulus and Poisson's ratio used for estimating BCJ material constants are listed in Table 3. The BCJ model parameters were fitted to the isothermal stress–strain data [17,27] at extreme temperatures at 293 and 993 K, Fig. 6. The BCJ material constants in Table 3 were obtained by tuning the magnitudes of each parameter following the method introduced in Section 4.1.1. The predictions of BCJ model with the determined material constants are consistent with the test data.

### 4.2.2. *Examination of the fitted material constants*

*Stress prediction at different temperatures*: The BCJ material constants determined by fitting the test data at 293 and 993 K were used to predict the flow stresses [17] at different temperatures of 573 and 773 K, Fig. 7. The predicted stress–strain curves clearly agree with the test data with reasonable accuracy, which shows that the obtained material constants can capture the

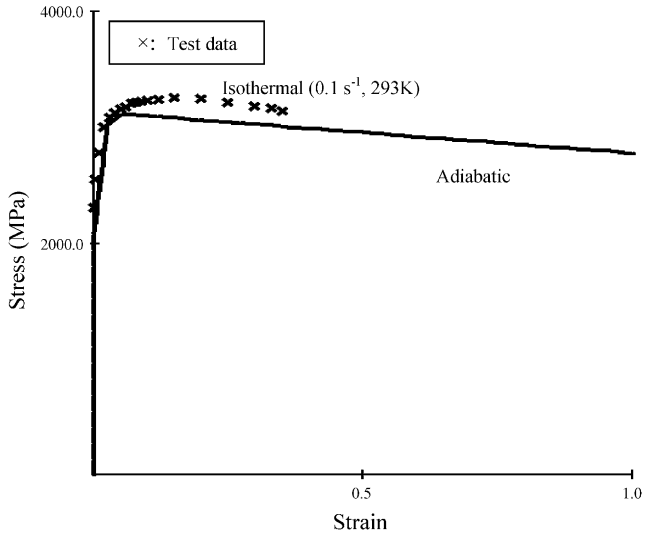


Fig. 8. Adiabatic curve by the BCJ model at 293 K of AISI 52100 (62 HRc) steel.

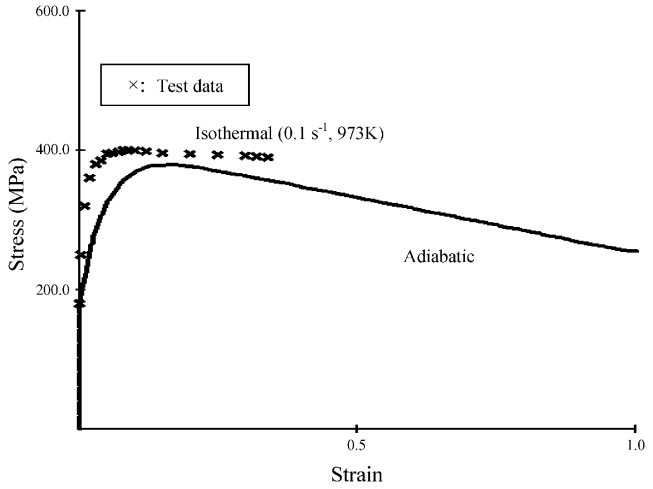


Fig. 9. Adiabatic curve by the BCJ model at 973 K of AISI 52100 (62 HRc) steel.

temperature effects on material flow stress and strain. The stress data at 293 and 993 K was also plotted in Fig. 7 for comparison.

*Adiabatic effect*: It is expected that large plastic deformations of this work material in hard machining will induce significant thermal softening due to adiabatic heating. With the determined material constants, the BCJ model predicted flow stresses, Figs. 8 and 9, clearly demonstrate thermal softening at large strains at 293 and 973 K. The thermal softening effect is much more significant at the high temperature. The prediction of adiabatic deformation further validates the capability of the BCJ model and the obtained material constants of AISI 52100 steel.

### 4.3. Aluminum 6061-T6

#### 4.3.1. Material constant estimation

Aluminum alloys are popular work materials for various forming, machining, especially high-speed machining operations. The US aluminum industry has been designated an "Industry of the Future" by the US Department of Energy. Because of the light weight of aluminum compared to steel, aluminum alloys are expected to grow substantially in the near future in automotive and aerospace industries. Therefore, the popular aluminum alloy 6061-T6 was used as a benchmark material in the study. A fundamental understanding of mechanical behavior of this material is particular important for the industries.

Aluminum 6061-T6 testing samples were solution heat treated at 540 °C for 0.5 h and artificially aged 205 °C for 3 h with nominal compositions given in Table 2. Quasi-static compression tests [10,19,28] and SHPB tests [29] were conducted to obtain the stress–strain data at different temperatures and strain rates. The BCJ material constants were obtained by fitting the BCJ model to the isothermal stress–strain data at two extreme temperatures of 293 and 673 K, Fig. 10. The temperature-dependent Young's modulus and Poisson's ratio used for fitting is listed in Table 3. The BCJ material constants were tuned after initial fitting by minimizing the fitting error. It can be seen that the obtained BCJ material constants allow the model predictions fit the test data very well.

#### 4.3.2. Examination of the fitted material constants

*Stress prediction at different temperatures:* Just like the BCJ material constants of Titanium Ti-6Al-4V and AISI 52100 alloy steels. The obtained material constants of aluminum 6061-T6 were examined by the model capability to predict flow stresses at different temperatures, strain rates, and adiabatic heating. With the determined BCJ material constants, the predicted flow

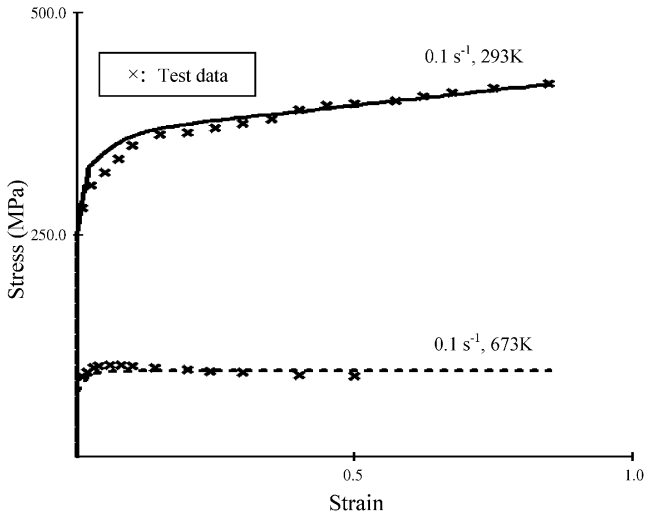


Fig. 10. Determination of BCJ material constants based on test data of AL 6061-T6 at extreme temperatures.

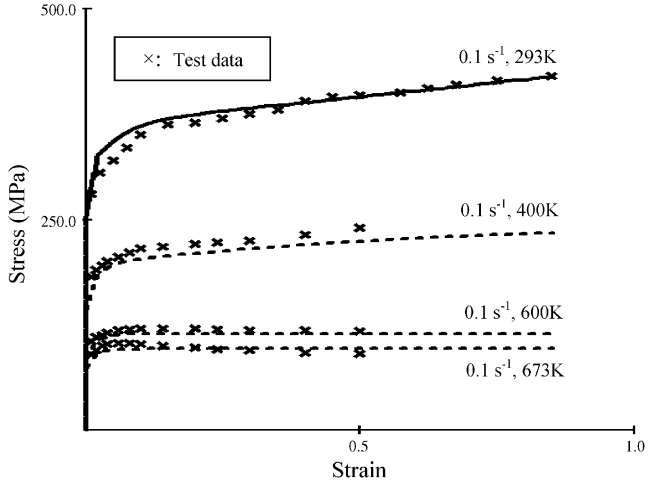


Fig. 11. BCJ model predictions of AL 6061-T6 at different temperatures.

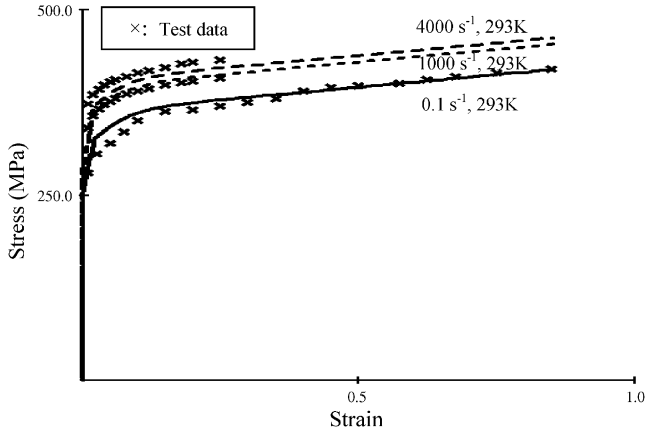


Fig. 12. BCJ model sensitivity to strain rate of AL 6061-T6.

stress–strain curves clearly agree with those of the test data at different temperatures of 400 and 600 K as shown in Fig. 11.

*Stress prediction at different strain rates*: Fig. 12 shows the sensitivity of model predictions using the material constants to strain rate. The selected strain rate varies from 0.1 to 4000 $s^{-1}$ that covers a large range of material deformations. The predicted flow stresses are consistent with the test data at different strain rates, which shows that the BCJ material constants capture the effects of strain rate on material flow stress.

*Adiabatic effect*: By incorporating a heat generation term, adiabatic flow stresses at 293 and 673 K were predicted, Figs. 13 and 14, with the BCJ material constants. As expected, the adiabatic heating at 293 K is small even at large strains. While the adiabatic-induced thermal softening is significant at high temperatures.

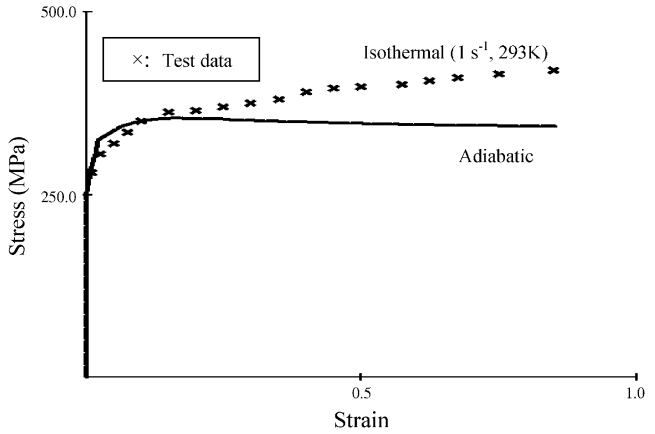


Fig. 13. Adiabatic curve by the BCJ model at 293 K of AL 6061-T6.

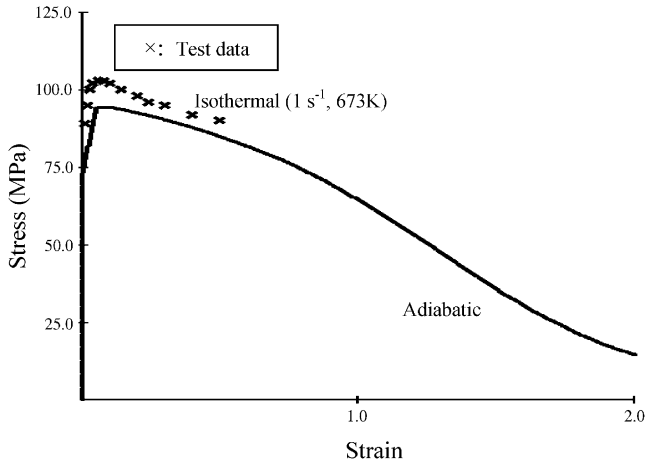


Fig. 14. Adiabatic curve by the BCJ model at 673 K of AL 6061-T6.

## 5. Discussion

The contributions of this paper can be summarized in three aspects: (a) compared with traditional JC or power law models, a different and more accurate approach was introduced to determine mechanical behavior in manufacturing processes, which provides manufacturing community a new perspective to understand material properties; (b) provide material properties of several important engineering materials widely used in industry for future use; and (c) demonstrate the capability of BCJ model to capture the history effect in large deformation processes. However, determining the material constants using the BCJ model is one thing, applying the determined data to an analytical or numerical analysis is quite another and is beyond scope of this study. The application of the determined material constants in simulating manufacturing processes will be the subject of additional investigation.

## 6. Conclusion

An internal state variable based BCJ model was explored to determine dynamic mechanical behavior of work materials with loading history effect in manufacturing processes. The use of internal state variables enables the prediction of strain, strain rate, temperature, and their history effects on material flow stress. The BCJ material constants were obtained by nonlinear least-square fitting the BCJ model to the isothermal stress–strain data. The capability of this approach was verified by three fundamental different materials, titanium Ti-6Al-4V, AISI 52100 steel, and aluminum 6061-T6. The research findings may be summarized as follows.

The BCJ material constants can be obtained by tuning the model parameters to fit the isothermal stress–strain data at extreme temperatures using the least-squares method.

With the determined BCJ material constants, the BCJ model predicts the flow stress with high fidelity at different temperatures, strains, strain rates, and their history effects.

The adiabatic heating-induced thermal softening can be predicted by incorporating a heat generation term. Thermal softening is significant at large strains and high temperatures.

## Acknowledgements

This research is based upon work supported by the National Science Foundation under Grant No. DMI-0447452. The assistance of Miss Christy Burton at Mississippi State University on determining material constants is greatly appreciated.

## References

[1] Alexander JM. On problems of plastic flow of materials. In: Sawczuk A, Bianchi G, editors. Plasticity today. London: Elsevier Applied Science Pub; 1985.
[2] Kalpakjian S. Manufacturing processes for engineering materials, 3rd ed. Menlo Park: Addison Wesley; 1997.
[3] Horstemeyer MF, Ramaswamy S, Negrete M. Using a micromechanical finite element parametric study to motivate a phenomenological macroscale model for void nucleation in aluminum with a hard second phase. Mechanics of Materials 2002;35:675–87.
[4] Johnson GR, Cook WH. A constitutive model and data for metals subjected to large strain, high strain rates and high temperatures. In: Proceedings of the seventh international symposium on ballistics. 19–21 April 1983.The Hague, The Netherlands. p. 541–47.
[5] Shirakashi T, Maekawa K, Usui E. Flow stress of low carbon steel at high temperature and strain rate, Part 1: property of incremental strain method in impact compression test with rapid heating and cooling systems. Bulletin of the Japan Society of Precision Engineering 1983;3:161–6.
[6] Zerilli FJ, Armstrong RW. Dislocation-mechanics-based constitutive relations for material dynamics calculations. Journal of Applied Physics 1987;61(5):1816–25.
[7] Michael EK, Sia N-N, Zhigang S, Gang B, Charles BJ, Catherine BL, Horacio E, Huajian G, Steve G, Peter G. New directions in mechanics. Mechanics of Materials 2005;37(2–3):231–59.
[8] Sia N-N, Wei-Guo Guo. Thermomechanical response of HSLA-65 steel plates: experiments and modeling. Mechanics of Materials 2005;37(2–3):379–405.
[9] Bammann DJ. Modeling temperature and strain rate dependent large deformation of metals. Applied Mechanics Review 1990;43(5):312–9.

[10] Bammann DJ, Chiesa ML, Johnson GC. Modeling large deformation and failure in manufacturing process.Theory of Applied Mechanics 1996;359–76.
[11] Kolsky H. An investigation of the material properties of materials at very high rates of loading. Proc Phy Soc B: Atomic and Molecular Physics 1949;62:676–700.
[12] Harding JE. Mechanical properties at high rates of strain. Proceedigs of second conference on the mechanical properties of materials at high rates of strain. 1979.Oxford, UK: Institute of Physics; 1979. p. 28–30.
[13] Duffy J. On the use of a torsional split Hopkinson bar to study rate effects in 1100-0 aluminum. Providence, RI: Division of Engineering, Brown University; 1970.
[14] Stevenson MG. Torsional Hopkinson bar tests to ensure stress–strain properties relevant to machining and high speed forming. Proceedings of the third NAMRC, Pittsburgh: Carnegie Press; 1975. p. 291–304.
[15] Olxey PLB. The mechanics of machining. Chichester: Ellis Horwood; 1989.
[16] Stevenson R. Study on the correlation of workpiece mechanical properties from compression and cutting tests. Journal of Mechanical Science and Technology 1997;1(1):67–79.
[17] Guo YB, Liu CR. Mechanical properties of hardened AISI 52100 steel in hard machining. ASME Journal of Manufacturing Science and Engineering 2002;124:1–9.
[18] Guo YB. Mechanical behavior characterization of the secondary shear zone in metal cutting. Transactions of NAMRI/SME 2002;XXX:423–30.
[19] Guo YB. An integrated method to determine the mechanical behavior of materials in metal cutting. Journal of Materials Processing Technology 2003;142:1–10.
[20] Usui E, Shirakashi T. Mechanics of machining—from 'descriptive' to 'predictive' theory, in on the art of cutting metals–75 years later. ASME PED-7, 1982. p. 13–35.
[21] Maekawa K, Shirakashi T, Usui E. Flow stress of low carbon steel at high temperature and strain rate. Part 2: flow stress under variable temperature and variable strain rate. Bulletin of the Japan Society of Precision Engineering 1983;17(3):167–72.
[22] Yoshino M, Shirakashi T. Flow-stress equation including effects of strain rate and temperature history. International Journal of Mechanical Science 1997;39(12):1345–62.
[23] Jaspers SPFC, Dautzenberg JH, Vellinga WP. Mechanical behavior of industrial alloys at high strain rate and temperature using the split hopkinson pressure bar. Proceedings of the sixth ISMQC IMEKO symposium. Metrology for quality control in production. 1998. p. 291–96.
[24] Chuzhoy L, DeVor RE, Kapoor SG, Beaudoin AJ, Bammann DJ. Machining simulation of ductile iron and its constituents. Part I: estimation of material model parameters and their validation. ASME Journal of Manufacturing Science and Engineering 2003;125:181–91.
[25] Horstemeyer MF, Lathrop J, Gokhale AM, Dighe M. Modeling stress state dependent damage evolution in a cast Al–Si–Mg aluminum alloy. Theory of Applied Mechanics 2000;33:31–47.
[26] Lee WS, Lin CF. High-temperature deformation behavior of Ti-6Al-4V alloy evaluated by high stain-rate compression tests. Journal of Materials Processing Technology 1998;75:127–36.
[27] Poulachon G, Moisan AL, Jawahir IS. Evaluation of chip morphology in hard turning using constitutive models and material property data. Proceedings of ASME-IMECE, New York, MED-12, 2002. p. 179–85.
[28] Horstemeyer MF, Matalanis MM, Sieber AM, Botos ML. Micromechanical finite element calculations of temperature and void configuration effects on void growth and coalescence. International Journal of Plasticity 2000;16:979–1015.
[29] Lee WS, Shyu JC, Chiou ST. Effect of strain rate on impact response and dislocation substructure of 6061-T6-aluminum alloy. Scripta Materialia 2000;42(1):51–6.